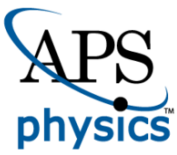

Quantum Hall Effect in Twisted Bilayer Graphene

Dong Su Lee, Christian Riedl, Thomas Beringer, A. H. Castro Neto, Klaus von Klitzing, Ulrich Starke, and Jurgen H. Smet

Phys. Rev. Lett. **107**, 216602 — Published 16 November 2011

DOI: 10.1103/PhysRevLett.107.216602

Quantum Hall Effect in Twisted Bilayer Graphene

Dong Su Lee,[1] Christian Riedl,[1] Thomas Beringer,[1] A. H. Castro Neto,[2,3] Klaus von Klitzing,[1] Ulrich Starke,[1] and Jurgen H. Smet[1]

[1]*Max-Planck-Institut für Festköperforschung, Heisenbergstr. 1, D-70569 Stuttgart, Germany*

[2]*Graphene Research Center and Department of Physics, National University of Singapore, Singapore, 117542*

[3]*Department of Physics, Boston University, 590 Commonwealth Avenue, Boston, Massachusetts 02215, USA*

Abstract

We address the quantum Hall behavior in twisted bilayer graphene transferred from the C-face of SiC. The measured Hall conductivity exhibits the same plateau values as for a commensurate Bernal bilayer. This implies that the eight-fold degeneracy of the zero energy mode is topologically protected despite rotational disorder as recently predicted. In addition, an anomaly appears. The densities at which these plateaus occur show a magnetic field dependent offset. It suggests the existence of a pool of localized states at low energy, which do not count towards the degeneracy of the lowest band Landau levels. These states originate from an inhomogeneous spatial variation of the interlayer coupling.

PACS numbers: 72.80.Vp 73.40.-c

The quantum Hall effect (QHE) in monolayer graphene is distinct from that of the traditional two-dimensional systems with massive electrons as a result of the linear dispersion and chiral nature of the Fermi Dirac charge carriers. Hall conductivity (σ_{xy}) quantization is observed at filling $\nu = \pm 2, \pm 6, \pm 10, \cdots$, where $\sigma_{xy} = (e^2/h)\nu$, because all Landau leves are fourfold degenerate. Moreover, the lowest Landau level (LL) is pinned at zero energy and its fourfold degeneracy is shared equally among holes and electrons [1, 2]. Bilayer graphene with AB-stacking on the other hand exhibits different Hall conductance plateaus: $\sigma_{xy} = (e^2/h)\nu_{tot}$, $\nu_{tot} = \pm 4, \pm 8, \pm 12, \cdots$ [3]. Charge carriers are still chiral, but near zero energy no longer follow a linear dispersion [4]. They occupy a parabolic band structure due to the electronic coupling between the two layers. Because two different orbital states have both zero energy, the zero energy mode is 8-fold degenerate. All other Landau levels are only fourfold degenerate as in a monolayer. When one layer is twisted by a small angle θ with respect to the other layer ($\theta = 0$: AB-stacking) the Dirac wavevector of the rotated layer is displaced to $K^\theta = K + \Delta K$, where $\Delta K = K \times 2\sin(\theta/2)$ [5, 6]. The states near the Dirac cone of each layer couple with amplitudes of order $t_\perp^\theta \sim 0.4\, t_\perp$ to states of energy $\pm\hbar v_F \Delta K$ of the opposing layer. Here $t_\perp$ is the interlayer hopping for unrotated layers and v_F the Fermi velocity. As a result, two Dirac cones appear at K and K^θ. The linear dispersion is preserved near zero energy, but the Fermi velocity is renormalized as compared to that in a monolayer [5, 7–9]. The linear dispersion has been experimentally demonstrated by Raman [10, 11] and angle resolved photoelectron spectroscopy [12]. Despite this similarity to a monolayer, the 8-fold degeneracy of the zero energy mode seen in commensurate Bernal graphene is topologically protected and not lost in bilayers with rotational disorder [13]. The recently observed electronic properties associated with a low-energy van Hove singularity at the saddle point in between the displaced Dirac cones [6] and the strain induced breaking of the local valley degeneracy [14] exemplify the richness of the physics in twisted bilayers. Despite these existing studies, the macroscopic transport behavior has remained largely unexplored. For instance QHE measurements were not yet reported.

For fully decoupled layers with equal density, the trivial behavior of two monolayers connected in parallel is expected and $\sigma_{xy} = 2(e^2/h)\nu_{single}$, $\nu_{single} = \pm 2, \pm 6, \pm 10, \cdots$ with ν_{single} the filling factor of a single layer or $\sigma_{xy} = (e^2/h)\nu_{tot}$ with total filling $\nu_{tot} = \pm 4, \pm 12, \pm 20$. The assumption of equal density in both layers may not hold in backgated samples, as the bottom layer will largely screen the applied electric field and an imbalance in the carrier

density is generated as the backgate voltage is tuned. The Hall conductivity in a system of decoupled layers with unequal densities ($n_{\rm top} \neq n_{\rm bottom}$) would closely resemble what has been reported on folded graphene [15] with two sets of superimposed Shubnikov-de Haas oscillations. The current applied through the system does not equally distribute among the two layers and the plateaus in $\sigma_{\rm xy}$ do not necessarily appear at integer values of e^2/h. Interestingly, neither of these unspectacular cases apply since the layers are not fully decoupled.

The twisted graphene layers were obtained by transferring material from epitaxially grown non-Bernal stacked graphite on the C-face of SiC [16, 17]. The graphene layers on the C-face of SiC are known to be stacked in a turbostratic fashion [18, 19] with angular distributions centered around $\pm 2.2^\circ$ and $30 \pm 2.2^\circ$ [8]. For the sake of completeness we point out that bilayers obtained from the Si-face of SiC are Bernal-stacked as confirmed recently in Ref. [20]. The epitaxial graphene growth was conducted by heating a 4H-SiC chip in a furnace with rf induction up to about 1300 °C [16]. Figure 1(a) shows an atomic force microscopy (AFM) image of the sample. There are wrinkles (marked by white arrows) on the surface. They are typical for epitaxial graphene on the C-face of SiC and on metallic surfaces [8, 21]. The growth of graphene occurs at high temperature. When one cools off the sample, the substrate contracts while graphene expands. Strain relaxation occurs through wrinkle or bubble formation [21]. An adhesive tape was used to transfer the graphene layers to a Si substrate covered with a 300 nm thick oxide layer [17]. Figure 1(b) displays an optical microscope image of the transferred flakes on the Si substrate. The optical contrast of the flakes was used to distinguish bilayer from monolayer and multilayer flakes [22]. Note that the transferred flake is not entirely flat (AFM image in Fig. 1(c)). It contains also small elevated regions. They are however somewhat distinct both in shape and height from those seen on the SiC starting wafer (compare Fig. 1(a) and (c)). These changes likely appear during the transfer onto the Si substrate and presumably strain, which is present between the SiC substrate and the graphene layers on top plays a role [14, 17]. After transfer, source and drain electrodes as well as four voltage probes in the geometry seen in Fig. 1(c) were fabricated with electron beam lithography and by evaporation of Cr/Au.

The turbostratic stacking of the transferred graphene layers was confirmed in Raman spectroscopy [10, 11]. Previous Raman studies demonstrated that the distinguishing feature between misoriented and commensurate Bernal bilayers is that for misoriented layers the 2D peak is not composed of four components, but only a single line as for monolayer

graphene [10, 11, 23]. The Raman data were acquired on the same sample used for quantum Hall studies and are plotted in Fig. 1(d). The 2D peak is located near 2700 cm^{-1} and fits to a single Lorentzian. It does not possess any shoulder structures as expected for twisted bilayers. We note for the sake of completeness that in all cases the 2D Raman peak is composed of a single component only, but the full-width-half-maximum (FWHM) of the 2D peak varies across the sample. This inhomogeneity is illustrated in the color rendition on the left. A narrowing of the 2D peak is also accompanied by a drop of the ratio of the 2D mode to G mode Raman strength (see right panel). Previous Raman studies on bilayers with rotational disorder have attributed this line width narrowing and amplitude increase to modified conditions for the double resonance process as the coupling between the graphene layers is varied and the electronic band structure changes [10, 11]. We conclude that the coupling in our sample is position dependent.

Figure 2 shows the Hall conductivity as a function of the density induced by the applied back-gate voltage, $V_{\rm bg}$. The total density is calculated from $n_{\rm app} = \alpha(V_{\rm bg} - V_{\rm N})$, where $\alpha = 7.2 \times 10^{10}$ $cm^{-2}V^{-1}$ and $V_{\rm N} = 18.5$ V is the offset voltage to reach charge neutrality. The coefficient α is known from studies on monolayer flakes using the identical substrate. The Hall conductivity is quantized to values equal to $\sigma_{\rm xy} = i \cdot e^2/h$ with $i = \pm 4, \pm 8, \cdots$. This sequence is identical as for a commensurate Bernal bilayer. This can not be understood if the two layers are considered fully decoupled. If the density is assumed identical in both layers, the $8e^2/h$ plateau cannot be explained. If the densities are unequal, Hall plateaus are no longer locked to integer multiples of e^2/h.

In order to understand why the quantum Hall behavior in a twisted bilayer, despite the linear dispersion at low energy, resembles that in Bernal stacked bilayers, the LL spectrum was calculated numerically using a continuum approximation [5] taking into account the lowest energy band of both layers. The energy dispersion reads: $E_{\pm}(p, \theta) = \pm(1/2m)\sqrt{p^4 - 2p_0^2 p^2 \cos^2\theta + p_0^4}$. Here, θ is the angle in momentum space ($p_{\rm x} = p\cos\theta$ and $p_{\rm y} = p\sin\theta$), $p_0^2 = 2m\Delta(\theta)$ and $\Delta(\theta)$ is the twist angle dependent van Hove energy [5, 6]. For the LL calculation we assumed $\Delta(\theta) = 0.1$ eV for $\theta = 2.2°$, the most frequently observed twist angle for epitaxial graphene layers grown on the C-face of SiC [8]. A detailed account of the calculations can be found in Ref. [13]. Fig. 2(b) displays the calculated Landau level spectrum. For comparison, the LL spectrum for a commensurate Bernal bilayer is also plotted in Fig. 2(c) [24, 25]. These spectra differ substantially. The gap between the zero energy

mode and the first higher or lower lying Landau level is much larger than the other level spacings. This is similar to the monolayer case in which the LL energy scales with $\sqrt{|n|}$ (n is the level index) due to the linear dispersion relation. At low B-fields when the Landau level energy is less than the van Hove energy (0.1 eV), energy levels are eightfold degenerate. In addition to the fourfold spin and valley degeneracy, there is an extra twofold degeneracy due to the Dirac point splitting in twisted bilayer graphene. This extra degeneracy is completely lifted at higher fields for all the LLs except for the zero mode. Even though the LL spectrum in Fig. 2b was calculated for a specific angle in the perturbative model, the general features of this spectrum remain valid even for other small twist angles less than $10 - 15°$. The Fermi velocity is renormalized and the Landau level energies merely rescale with the twist angle dependent van Hove energy $E_{\mathrm{vH}} = (1/2)\hbar v_{\mathrm{F}}\Delta K - t_{\perp}^{\theta}$. Only at larger angles the Fermi velocity is almost the same as for monolayer graphene and the layers are decoupled as shown in Ref. [26]. Under these circumstances, we would expect however a strong density imbalance between top and bottom layer as a result of screening of the backgate voltage by the bottom layer. This would cause Hall conductance quantization at plateaus which are in general no longer integer multiples of the conductance quantum. Hence, we conclude that the twist angle here is small and the perturbative model is justified.

The eightfold degeneracy of the zero mode is topologically protected in the entire range of B [13]. Hence, for high fields the degeneracy of the LLs is the same as that for Bernal stacked bilayer: eightfold for the zero energy mode and fourfold for others. Our observation of the $\nu = 4$ and 8 quantum Hall plateau provides experimental evidence for this theoretical prediction. In experiment, the extra two-fold degeneracy for the non-zero energy Landau levels has already been lifted at 5 T. We note the absence of the $\nu = 12$ plateau for holes. There are theoretical studies which can explain the absence of the $\nu = 12$ plateau. In these studies the interlayer hopping is continuously tuned [27]. Also, a level crossing of the $n = 2$ and $n = 3$ LL has been reported [28], which would cause a skipping of the $\nu = 12$ plateau in the σ_{xy} curves. Even though not fully developed the Hall conductivity shows signs for $\nu = 16$ and 20 plateaus.

More surprising are the carrier densities at which the Hall conductivity plateaus appear. In the case of a commensurate Bernal bilayer, the transition of the Hall conductivity from $4e^2/h$ to $8e^2/h$ occurs at a density near $6eB/h$. Subsequent Hall plateau transitions are equidistantly spaced with a period of $4eB/h$ because of the fourfold degeneracy of the non-

zero energy Landau levels. In the measured data on the twisted bilayer, despite a plateau sequence following that of a Bernal bilayer, the transition from $4e^2/h$ to $8e^2/h$ takes place at a much larger density than $6eB/h$. Fits of the Hall conductivity at high density have been included as dashed lines in Fig. 2(a) and illustrate that these fits do not cross zero density at zero Hall conductivity. For example, at a field of 5 T, the Hall conductivity transition from $4e^2/h$ to $8e^2/h$ appears at $\sim 1.8 \times 10^{12}$ cm^{-2} although it is expected at $6eB/h \sim 0.7 \times 10^{12}$ cm^{-2}. In Fig. 3(a), the Hall conductivity is replotted by rescaling the $n_{\rm app}$-abscissae in units of $4eB/h$. The dashed line marks the position of Hall conductivity transitions for a Bernal bilayer Hall plateau sequence. Clearly, the transition from $4e^2/h$ to $8e^2/h$ is "delayed". For subsequent Hall plateau transitions no additional significant shifts are observed. This behavior suggests the existence of a pool of localized states, which do not contribute to the Hall conductivity. They also do not count towards the degeneracy of the zero'th energy mode, but need to be filled in addition to all states of the zero energy mode before the next Landau level is broached. Apparently, the density induced by the back-gate is composed of two contributions: $n_{\rm app} = n_{\rm tr} + n_{\rm loc}$. Here $n_{\rm tr}$ is the carrier density that contributes to Hall transport and $n_{\rm loc}$ is the amount of localized charge carriers that does not contribute to the measured Hall conductivity. When the external applied magnetic field is altered, also $n_{\rm loc}$ changes. The localized charge $n_{\rm loc}$ has been extracted as shown in Fig. 3(a) by subtracting $6eB/h$ from the density at which the Hall conductivity changes from $4e^2/h$ to $8e^2/h$. It follows a $\sqrt{B}$ dependence (Fig. 3(b)), whereas the Landau level degeneracy scales linearly with B. The extracted $n_{\rm loc}$ for holes is not significantly different from that for electrons.

We attribute this unusual quantum Hall behavior to a random spatial variation of the coupling between the two layers. Imagine a disordered system where those regions where the graphene layers are weakly coupled form a continuous sea. Islands where the graphene layers are strongly coupled are dispersed within this sea. Consider the extreme case, where the domains with strong coupling possess the Landau level spectrum of a commensurate Bernal bilayer, while in the weakly coupled region the spectrum resembles that of a monolayer in the sense that the Landau level spacing at low energies is much larger. These two spectra are plotted in Fig. 3(c). For the sake of simplicity we took the spectrum of a monolayer, although we still have some coupling (The fully decoupled scenario would be in contraction with the observed Hall data.) The more closely spaced levels in the domains with strong interlayer coupling must be filled before the second Landau level of the region with weak

interlayer coupling gets filled. The charge carriers occupying these domains with strong interlayer coupling are isolated or localized and do not contribute to the Hall conductivity. If one assumes a parabolic band for these domains, their density can be approximated as $n_{\mathrm{loc}} = (A_{\mathrm{coupled}}/A_{\mathrm{tot}}) \cdot D_{\mathrm{coupled}} \cdot \Delta E$. Here A_{tot} and A_{coupled} are the total sample area and the area with strong interlayer coupling and D_{coupled} is the constant density of states at $B = 0$ in the region for strong interlayer coupling. ΔE is the energy separation between the zero energy mode and the second Landau level of the weakly coupled region. This energy gap scales with the $\sqrt{B}$ and hence also n_{loc} grows as $\sqrt{B}$. Even though this model is certainly oversimplified, it captures the dependence of n_{loc} on B observed in experiment (Fig. 3c).

Remains the question whether other evidence is available for a spatially inhomogeneous coupling strength between the layers. The Raman data in Fig. 1(c) points to the existence of domains with different electronic structures. A spatial variation of the electronic structure has recently also been observed in scanning tunneling microscopy studies in which the local density of states was measured on the same type of material, i.e. epitaxial graphene layers on the C-face of SiC [14]. These studies too revealed regions which behave as a commensurate Bernal bilayer and the properties of other areas resembled those of a weakly coupled bilayer. It was argued that strain issues during epitaxial growth and subsequent cool down are responsible for this inhomogeneous behavior. Note that in twisted layers the local stacking will vary periodically for a discrete set of commensurate angles. At such commensurate twist angles, a Moiré pattern with a unit cell determined by the twist angle emerges. The periodic nature of this spatial variation prevents however the formation of localized states in view of Bloch's theorem when the coherence length exceeds the characteristic length of the unit cell. Hence, the observed localized states require that we invoke a spatially aperiodic or inhomogeneous variation of the electronic coupling between the layers. Even though a twisted layer with an incommensurate angle would be sufficient, we believe that strain relaxation combined with the softness of graphene in the third dimension is more likely at the origin of the inhomogeneous spatial variation of the layer coupling.

In conclusion, we have addressed the QHE in twisted bilayer graphene flakes transferred from epitaxial graphene grown on the C-face of SiC. The measured Hall conductivity exhibits the same plateau values as for a commensurate Bernal bilayer. This implies that the eight-fold degeneracy of the zero energy mode is topologically protected despite rotational disorder as recently predicted. In addition, an anomaly appears. The densities at which these plateau

occur show a B-dependent offset. This has been attributed to reservoirs of localized states which form as a result of a spatial variation of the interlayer coupling.

We acknowledge discussions with M. Nakamura and T. Ando. We thank W. Dietsche, Y. Yoon, A. Köhler and M. Hagel for sample growth and preparation. We are grateful for financial support from the priority programm Graphene (DFG). AHCN acknowledges DOE grant DE-FG02-08ER46512 and ONR grant MURI N00014-09-1-1063.

---

[1] K. S. Novoselov*et al.*, Nature **438**, 197 (2005).

[2] Y. B. Zhang *et al.*, Nature **438**, 201 (2005).

[3] K. S. Novoselov *et al.*, Nat. Phys. **2**, 177 (2006).

[4] E. McCann and V. I. Fal'ko, Phys. Rev. Lett. **96**, 086805 (2006).

[5] J. Lopes dos Santos, N. M. R. Peres, and A. H. Castro Neto, Phys. Rev. Lett. **99**, 256802 (2007).

[6] G. H. Li *et al.*, Nat. Phys. **6**, 44 (2010).

[7] S. Latil, V. Meunier, and L. Henrard, Phys. Rev. B **76**, 201402 (2007).

[8] J. Hass *et al.*, Phys. Rev. Lett. **100**, 125504 (2008).

[9] M. -Y. Choi, Y. -H. Hyun, Y. Kim, arXiv:1105.4551 (2011).

[10] Z. H. Ni *et al.*, Phys. Rev. B **77**, 235403 (2008).

[11] P. Poncharal *et al.*, Phys. Rev. B **78**, 113407 (2008).

[12] M. Sprinkle et al., Phys. Stat. Sol. **3**, A91 (2009).

[13] R. de Gail *et al.*, Phys. Rev. B **84**, 045436 (2011).

[14] D. L. Miller *et al.*, Nat. Phys. **6**, 811 (2010).

[15] H. Schmidt et al., Appl. Phys. Lett. **93**, 172108 (2008).

[16] K. V. Emtsev *et al.*, Nat. Mater. **8**, 203 (2009).

[17] D. S. Lee *et al.*, Nano Lett. **8**, 4320 (2008).

[18] L. B. Biedermann *et al.*, Phys. Rev. B **79**, 125411 (2009).

[19] F. Varchon *et al.*, Phys. Rev. B **77**, 165415 (2008).

[20] K. Lee *et al.*, Nano Lett. in press.

[21] N. Levy *et al.*, Science **329**, 544 (2010).

[22] P. Blake et al., Appl. Phys. Lett. **91**, 063124 (2007).

[23] A. C. Ferrari *et al.*, Phys. Rev. Lett. **97**, 187401 (2006).

[24] J. M. Pereira, F. M Peeters, and P. Vasilopoulos, Phys. Rev. B **76**, 115419 (2007).

[25] E. A. Henriksen *et al.*, Phys. Rev. Lett. **100**, 087403 (2008).

[26] G. Trambly de Laissardière, D. Mayou, and L. Magaud. Nano Lett. **10**, 84 (2010).

[27] M. Nakamura, L. Hirasawa, and K. I. Imura, Phys. Rev. B **78**, 033403 (2008).

[28] V. M. Apalkov and T. Chakraborty, Phys. Rev. B **84**, 033408 (2011).

FIG. 1: (a) An AFM image of a few-layer epitaxial graphene grown on C-face of SiC. (b) An optical microscope image of the graphene flakes mechanically exfoliated from SiC to SiO_2. (c) A representative AFM image of the fabricated devices. (d) Spatial resolved Raman spectra measured for the twisted bilayer flake transferred to SiO_2 substrate. The incident light is generated by a 488 nm Ar^+ laser and the spot size is around 400 nm. The left panel shows a map of the FWHM of the 2D Raman peak). The Raman data in the right panel are the representative spectra for the different regions seen in the color rendition.

FIG. 2: (a) Hall conductivity as a function of $n_{\rm app}$. (b-c) LL spectra of (b) twisted bilayer graphene and of (c) Bernal stacked bilayer graphene. The degeneracy of the energy levels is color coded: red corresponds to 8-fold degenerate and black to 4-fold degenerate.

FIG. 3: (a) The Hall conductivity as a function of charge carrier density rescaled by $4eB/h$. Black dashed line shows the Hall conductivity expected for Bernal-stacked bilayer graphene for a comparison. (b) The localized charge carrier density $n_{\rm loc}$ for holes (open circles) and for electrons (solid circles) as a function of $\sqrt{B}$. Dashed line is the linear fit of the data for holes. (c) Schematic illustration of the LLs for the regions where the interlayer coupling is strong and weak. The energy gap between the zero mode and the next LL, E_{01} of the decoupled region is shaded by gray.

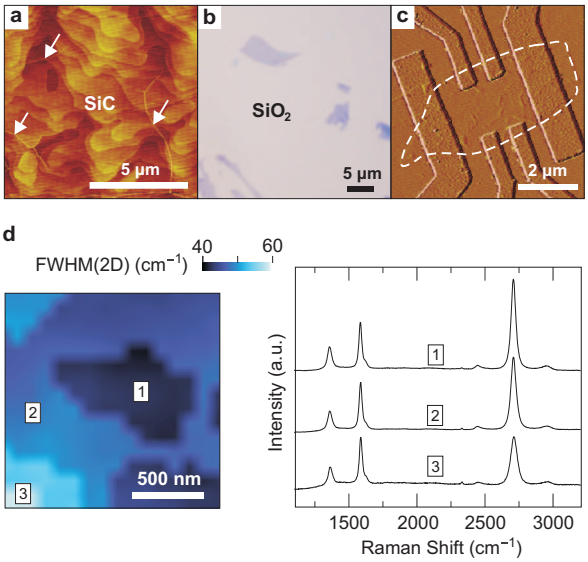

Figure 1 LF13836 26Sep2011

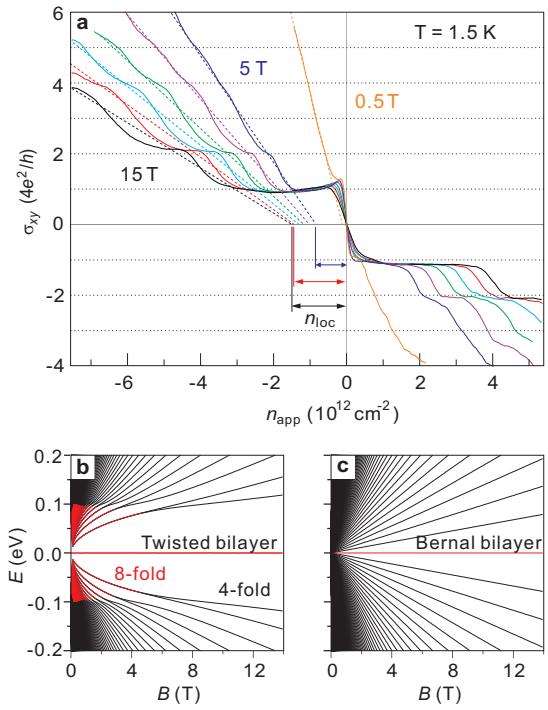

Figure 2 LF13836 26Sep2011

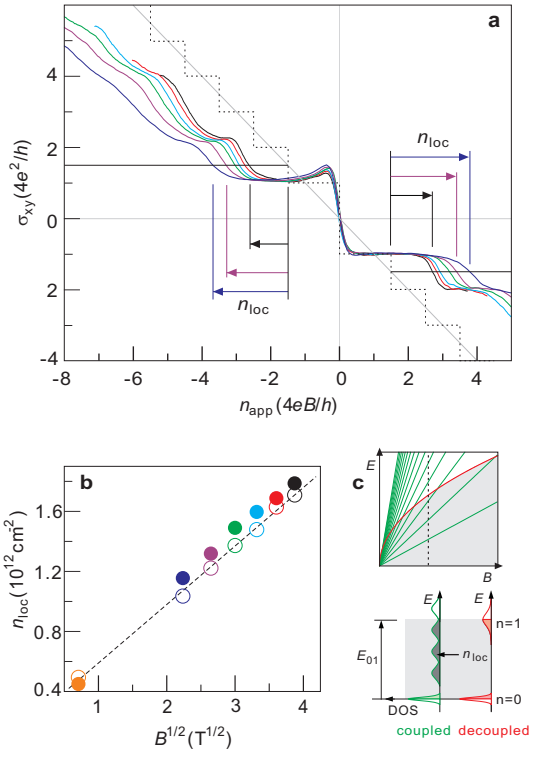

Figure 3 LF13836 26Sep2011